

Phase structure evolution and coercivity mechanism of high-Co containing permanent magnets

Min Huang(黄敏), Yong Ding(丁勇), Zhihe Zhao(赵之赫), Chunguo Wang(王春国), Bo Zhou(周波), Lei Liu(刘雷), Yingli Sun(孙颖莉), and Aru Yan(闫阿儒)

Citation: Chin. Phys. B, 2024, 33 (**11**): 117503. DOI: 10.1088/1674-1056/ad6b82
Journal homepage: http://cpb.iphy.ac.cn; http://iopscience.iop.org/cpb

What follows is a list of articles you may be interested in

Gate-voltage control of alternating-current-driven skyrmion propagation in ferromagnetic nanotrack devices

Xin-Yi Cai(蔡心怡), Zhi-Hua Chen(陈志华), Hang-Xiao Yang(杨航霄), Xin-Yan He(何鑫岩), Zhen-Zhen Chen(陈珍珍), Ming-Min Zhu(朱明敏), Yang Qiu(邱阳), Guo-Liang Yu(郁国良), and Hao-Miao Zhou(周浩淼)
Chin. Phys. B, 2023, 32 (**6**): 067502. DOI: 10.1088/1674-1056/acb420

Micromagnetic study of magnetization reversal in inhomogeneous permanent magnets

Zhi Yang(杨质), Yuanyuan Chen(陈源源), Weiqiang Liu(刘卫强), Yuqing Li(李玉卿), Liying Cong(丛利颖), Qiong Wu(吴琼), Hongguo Zhang(张红国), Qingmei Lu(路清梅), Dongtao Zhang(张东涛), and Ming Yue(岳明)
Chin. Phys. B, 2023, 32 (**4**): 047504. DOI: 10.1088/1674-1056/ac9359

Three- and two-dimensional calculations for the interface anisotropy dependence of magnetic properties of exchange-spring $Nd_2Fe_{14}B/\alpha$-Fe multilayers with out-of-plane easy axes

Qian Zhao(赵倩), Xin-Xin He(何鑫鑫), Francois-Jacques Morvan(李文瀚), Guo-Ping Zhao(赵国平), Zhu-Bai Li(李柱柏)
Chin. Phys. B, 2020, 29 (**3**): 037501. DOI: 10.1088/1674-1056/ab69e9

Thermal stability, crystallization, and magnetic properties of FeNiBCuNb alloys

Zhe Chen(陈哲), Qian-Ke Zhu(朱乾科), Shu-Ling Zhang(张树玲), Ke-Wei Zhang(张克维), Yong Jiang(姜勇)
Chin. Phys. B, 2019, 28 (**8**): 087502. DOI: 10.1088/1674-1056/28/8/087502

Coercivity mechanisms in nanostructured permanent magnets

G P Zhao(赵国平), L Zhao(赵莉), L C Shen(沈来川), J Zou(邹静), L Qiu(邱雷)
Chin. Phys. B, 2019, 28 (**7**): 077505. DOI: 10.1088/1674-1056/28/7/077505

Phase structure evolution and coercivity mechanism of high-Co containing permanent magnets

Min Huang(黄敏)[1,2], Yong Ding(丁勇)[1,2,†], Zhihe Zhao(赵之赫)[1,2], Chunguo Wang(王春国)[1,2], Bo Zhou(周波)[1,2], Lei Liu(刘雷)[1,2], Yingli Sun(孙颖莉)[1,2,‡], and Aru Yan(闫阿儒)[1,2]

[1] *CISRI & NIMTE Joint Innovation Center for Rare Earth Permanent Magnets, CAS Key Laboratory of Magnetic Materials and Devices, Zhejiang Province Key Laboratory of Magnetic Materials and Application Technology, Ningbo Institute of Materials Technology and Engineering, Chinese Academy of Sciences, Ningbo* 315201, *China*

[2] *University of Chinese Academy of Sciences, Beijing* 100049, *China*

(Received 7 April 2024; revised manuscript received 21 July 2024; accepted manuscript online 6 August 2024)

The phase structure and magnetic properties of high-Co containing permanent magnets with high thermal stability have been systematically studied in this work. It is abnormal that the coercivity of annealed samples was slightly lower than that of sintered samples, while the coercivity was usually enhanced after annealing in conventional Nd–Fe–B samples. Further analysis showed that in addition to $RE_2(Fe,Co)_{14}B$ main phase and RE-rich grain boundary phase, there were also new Co-rich magnetic phases located in the grain boundary. During annealing, the phase structures of high-Co containing magnets were readjusted, especially the increasing Co-rich magnetic phase and emerging RE-rich particles precipitated from the main phase. Eventually, the isolated RE-rich particles would act as the pinning center of the domain wall movement in demagnetization process. It was confirmed that the coercivity of annealed high-Co containing magnets was controlled by both nucleation and pinning. Pinning mechanism can partially compensate for the weakening of magnetic isolation due to increased Co-rich magnetic phase, which explained the moderate decrease in coercivity of annealed high-Co containing magnets. The discovery of new coercivity mechanism contributed to in-depth understanding of high-Co containing magnets.

Keywords: Co-rich phase, pinning, coercivity mechanism, high-Co containing magnets

PACS: 75.50.Ww, 75.60.–d, 75.60.Jk **DOI:** 10.1088/1674-1056/ad6b82

1. Introduction

Due to superior magnetic properties, sintered Nd–Fe–B magnets have attracted much attention and been widely used in hybrid and electric vehicles, wind power generators, electronic appliances, etc.[1–5] With the rapid development of modern industries, both excellent magnetic properties and enhanced thermal stability of permanent magnets at higher operating temperatures are required for extensive applications.[2,6] However, the relatively low Curie temperature of 312 °C in pure ternary Nd–Fe–B system is a primary drawback impeding their operations at elevated temperatures.[7,8] It is strongly desired to develop higher thermal stability and reliability Nd–Fe–B magnets to meet the fast-growing demand for high-temperature permanent magnets. Thus, improving Curie temperature while maintaining high intrinsic coercivity has become a focus of current research in conventional Nd–Fe–B magnets.

Compared with $Tb_2Fe_{14}B$ ($T_c = 620$ K) and $Dy_2Fe_{14}B$ ($T_c = 598$ K), Curie temperature of $Nd_2Co_{14}B$ is surprisingly up to 1000 K.[9–11] It was reported that the temperature coefficients of remanence and coercivity almost decreased linearly with increasing Co substitution in the range of 1%–10% (atomic fraction).[12–14] Adequate Co substitution would ensure comparable temperature stability.[15,16] However, on the one hand, the anisotropy field and the saturation magnetization of $Nd_2Co_{14}B$ phase were significantly lower than those of $Nd_2Fe_{14}B$ phase.[3,9] On the other hand, the addition of excessive Co elements inevitably entered the grain boundary, bringing about some variation of phase constituent. Relevant studies have confirmed that there may be complicated phases including $RE(FeCo)_2$, RE_2Co_{17} and $RE(FeCo)_3$ appearing in high-Co containing Nd–Fe–B magnets,[17,18,20] which were proved to be magnetic with Curie points above room temperature. It is the occurrence of these magnetic grain boundary phases that significantly weakened the magnetic properties, especially the coercivity of high-Co containing Nd–Fe–B system.

In order to reduce the deterioration of coercivity caused by increasing Co substitution, appropriate heavy rare earths are usually added for performance balancing. Many scholars tried to optimize the ratio of HRE to Co in order to obtain the best stability matching magnetic properties.[15,21,22] The existing research focused more on the preparation of high thermostability magnets, and seldom studied the mechanism of high-Co containing Nd–Fe–B system in detail. According to Xu *et al.*'s studies,[21] the presence of $(Nd,Dy)(Fe,Co)_3$ phase in Co13 magnet with Curie temperature of 454 °C led to reduced coercivity. Zhang *et al.* believed that Co-rich phase

†Corresponding author. E-mail: dingyong@nimte.ac.cn
‡Corresponding author. E-mail: yinglisun@nimte.ac.cn

© 2024 Chinese Physical Society and IOP Publishing Ltd

components were related to heat-treated states in high-Co containing Nd–Fe–B magnets with 13 wt.%.[17] Co substitution. $RE(Fe,Co)_2$ Laves phase tended to occur under water quenching condition, while $RE_2(Fe,Co)_{17}$ appeared easily in air cooling condition. Based on these adverse effects, an appropriate method was explored to eliminate or reduce Co-rich phase. Jin *et al.* adopted dual-alloy process to inhibit the formation of Co-rich phase, thereby maximizing coercivity while ensuring the same stability.[18] Zhang *et al.* improved the distribution uniformity of Co at the grain boundary with $Pr_{80}Cu_{20}$ addition in high-Co containing magnets, which effectively eliminated Co-rich phase, and increased its coercivity.[22] Xu *et al.* found that Ga addition can effectively transform soft-magnetic Laves phase into paramagnetic $(Nd,Dy)(Fe,Co,Ga)_2$ phase, improving grain boundary wettability.[23] In recent years, Wu *et al.* found that the underlying mechanism of deterioration in magnetic property of high-Co containing magnets was overneglected.[24] A lot of research was done on the phase formation, resultant microstructure and their correlation with the coercivity mechanisms of high-Co containing hot-compacted magnets, which has brought us much inspiration.[19,24,25] Up to now, the mechanism of complicated Co-rich constituent on coercivity is still inexplicit in high-Co containing sintered Nd–Fe–B magnets.

In this work, conventional Nd–Fe–B magnets and high-Co containing magnets were obtained by the same preparation process. Among these, a conventional Nd–Fe–B magnet was used as a reference. The phase structure evolution of a high-Co containing magnet and its relationship with magnetic properties during annealing were systematically studied. Eventually, the internal effect mechanism of grain boundary phase on coercivity was elucidated.

2. Experimental details

Strip-casting flakes with a high-Co-containing component $(NdPr)_{28}Tb_3Co_{22}M_{0.45}B_{0.94}Fe_{bal}$ (M = Cu, Al, Zr) were prepared by induction melting under Ar atmosphere. After hydrogen decrepitation and jet milling, the fine powders were produced with an average particle size of 3 μm. Subsequently, these powders were aligned in a mold and pressed in a magnetic field of 2 T. The aligned magnets were further compressed via isostatic pressing at 200 MPa. Finally, the green compacts were sintered at 1050 °C–1070 °C for 2 h in a vacuum atmosphere ($< 3 \times 10^{-3}$ Pa), and high-Co-containing magnets in sintered state were obtained (hereafter named as sintered Co22 sample). Then, post-sinter annealing (PSA) was further carried out. The choice of consecutive PSA was conducted at 900 °C for 2 h (1st annealing) and 450 °C–720 °C for 4 h (second annealing) (hereafter named as annealed Co22 sample). As a reference, convention Nd–Fe–B magnets with the nominal composition of $(NdPr)_{31}Co_{1.5}M_{0.45}B_{0.94}Fe_{bal}$ (M = Cu, Al, Zr) were prepared in the same sintering process (hereafter named the sintered Co1.5 sample). In contrast, subsequent consecutive PSA was only conducted at 900 °C for 2 h and 500 °C for 4 h (hereafter named the annealed Co1.5 sample).

The samples for magnetic properties tests were cylinders with a size of $\Phi 10 \times 10$ mm^3. The demagnetization curves of magnets in different states at room temperature were measured by a NIM-500C hysteresis-graph analyzer system. The initial magnetization curves and minor hysteresis loops were obtained by vibrating sample magnetometer (VSM, LakeShore-7410). To identify the phase compositions, x-ray diffractometer (XRD-D8 ADVANCE) was performed on the powder samples, and a Rietveld refinement by Fullprof software further confirmed the ratio of constituent phase. The melting points of different phases were analyzed by differential scanning calorimeter (DSC, NETZSCH 214). Scanning electron microscopy (SEM, FEI Quanta FEG 250) with an energy dispersive x-ray spectrometer (EDS) was used for microstructure observation and element analysis. The detailed nanostructure was investigated by transmission electron microscopy (TEM; Talos F200X) equipped with an EDS signal detection. Meanwhile, *in situ* magnetic domain observation was carried out by Lorentz transmission electron microscopy (LTEM, ThemoFisher Talos F200x).

3. Results and discussion

Figure 1(a) shows the demagnetization curves of sintered and annealed magnets with different Co content, and the corresponding magnetic properties are listed in Table 1. First, compared with sintered samples, it is found that B_r and $(BH)_{max}$ of annealed samples varied very slightly. However, the variation in coercivity of corresponding magnets with different Co content is completely different. It is indicated that the coercivity of Co1.5 sample increases substantially to 12.94 kOe with an obvious increment of 3.51 kOe after annealing. Nevertheless, the coercivity of Co22 sample with post-sintering treatment decreases to 12.96 kOe, which shows moderate reduction of 1.8 kOe compared with its sintered sample. Figure 1(b) further complements the coercivity values of high-Co-containing magnets over a wider annealing temperature range. On the whole, with increasing annealing temperature, coercivity first increases and then decreases. Even at the optimum annealing temperature, the $(H_{cj})_{max}$ of magnets is not enhanced significantly or even slightly lower than that of sintered magnets. However, it was evident that the temperature coefficients of remanence and coercivity of annealed Co22 sample increased from −0.104 %/°C and −0.649 %/°C to −0.067 %/°C and −0.568 %/°C, respectively, as shown in Figs. 1(c) and 1(d). Higher magnetic stability is obtained in high-Co-containing magnets.

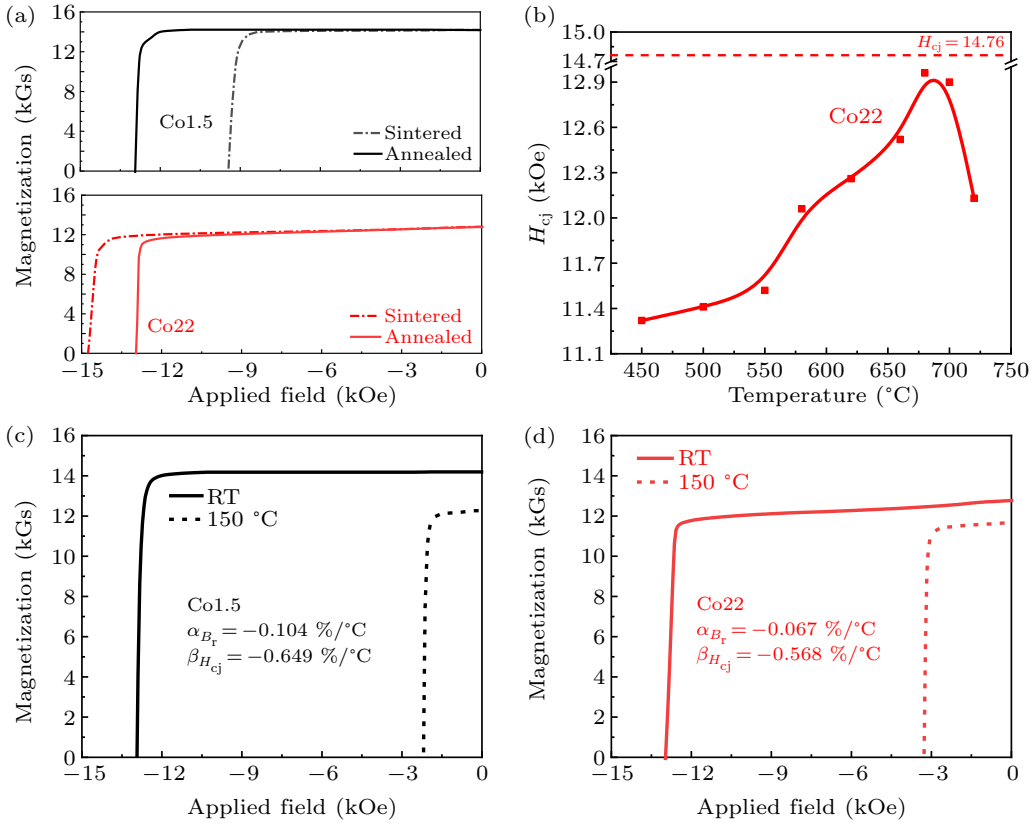


Fig. 1. Demagnetization curves at sintered and annealed states of Co1.5 and Co22 samples (a), the dependence of coercivity on second annealing temperature for Co22 sample (b), demagnetization curves at room temperature and 150 °C for annealed Co1.5 sample (c) and annealed Co22 sample (d).

Table 1. The B_r, H_{cj} and $(BH)_{max}$ for sintered and annealed Co1.5 and Co22 samples.

Samples		B_r (kGs)	H_{cj} (kOe)	$(BH)_{max}$ (MGOe)
Co1.5	sintered	14.20	9.43	49.55
	annealed	14.17	12.94	49.98
Co22	sintered	12.81	14.76	38.24
	annealed	12.79	12.96	37.74

According to the above, it was confirmed that moderate reduction of coercivity did occur in annealed high-Co-containing magnets, which is totally different from conventional Nd–Fe–B magnets.[26] It is obvious that the introduction of large quantities of Co elements has brought about some substantial difference in new-style high-Co-containing Nd–Fe–B magnets, which may be related to its internal phase structure and coercivity formation mechanism.

In order to further understand the inherent structural characteristics, high-Co-containing magnets (Co22 samples) were selected as main research objects in the later section. Through the abnormal performance differences in sintered sample and the optimal annealed sample, the internal relationship between the microstructure and the performance mechanism is systematically explored in new-style high-Co-containing Nd–Fe–B magnets.

Figure 2(a) presents the XRD patterns of powder samples in Co22 magnets under different heat-treated conditions. The results show that both sintered and annealed samples are composed of 2:14:1 main phases and two intergranular phases ($RE(Fe,Co)_2$ phases and RE-rich phases). No new diffraction peaks were found in annealed magnet, which indicates that no phase transition occurs during annealing. It is well known that conventional Nd–Fe–B magnets were composed of 2:14:1 main phases and RE-rich phases. However, in high-Co-containing magnets, due to the introduction of too much Co, on the one hand, Co entered the main phase and replaced Fe element partly, forming $RE_2(Fe,Co)_{14}B$ phase, which may result in a reduction in lattice parameters of main phase. Actually, the shift of the main peak towards lower angles in annealed sample can be clearly observed in the local magnification. Following the Bragg equation $2d\sin\theta = n\lambda$,[27] it is indicated that the crystal plane spacings and lattice parameters increased,[28] which may imply that part of Co element came out of the main phase after annealing. On the other hand, excess Co would enter the grain boundary phase in high-Co-containing magnets, partially changing the composition of the original RE-rich phase in conventional Nd–Fe–B magnets. At the same time, a new ferromagnetic Co-rich $RE(Fe,Co)_2$ phase is formed. Figure 2(b) lists the Rietveld refinements for each sample, and the refined results of XRD patterns are also shown in Fig. 2(c). It is found that the content of the three component phases is adjusted slightly after annealing in high-

Co-containing magnets. The volume fraction of main phases decreased from 95.27 wt.% to 93.25 wt.%, while the content percentage of RE-rich intergranular and RE(Fe,Co)$_2$ phases increased from 1.68 wt.% and 3.05 wt.% to 2.17 wt.% and 4.58 wt.%, respectively. In addition, the refined results also show that the lattice parameters of the main phase in the annealed sample slightly increased, which corresponds well with the movement of diffraction peaks.

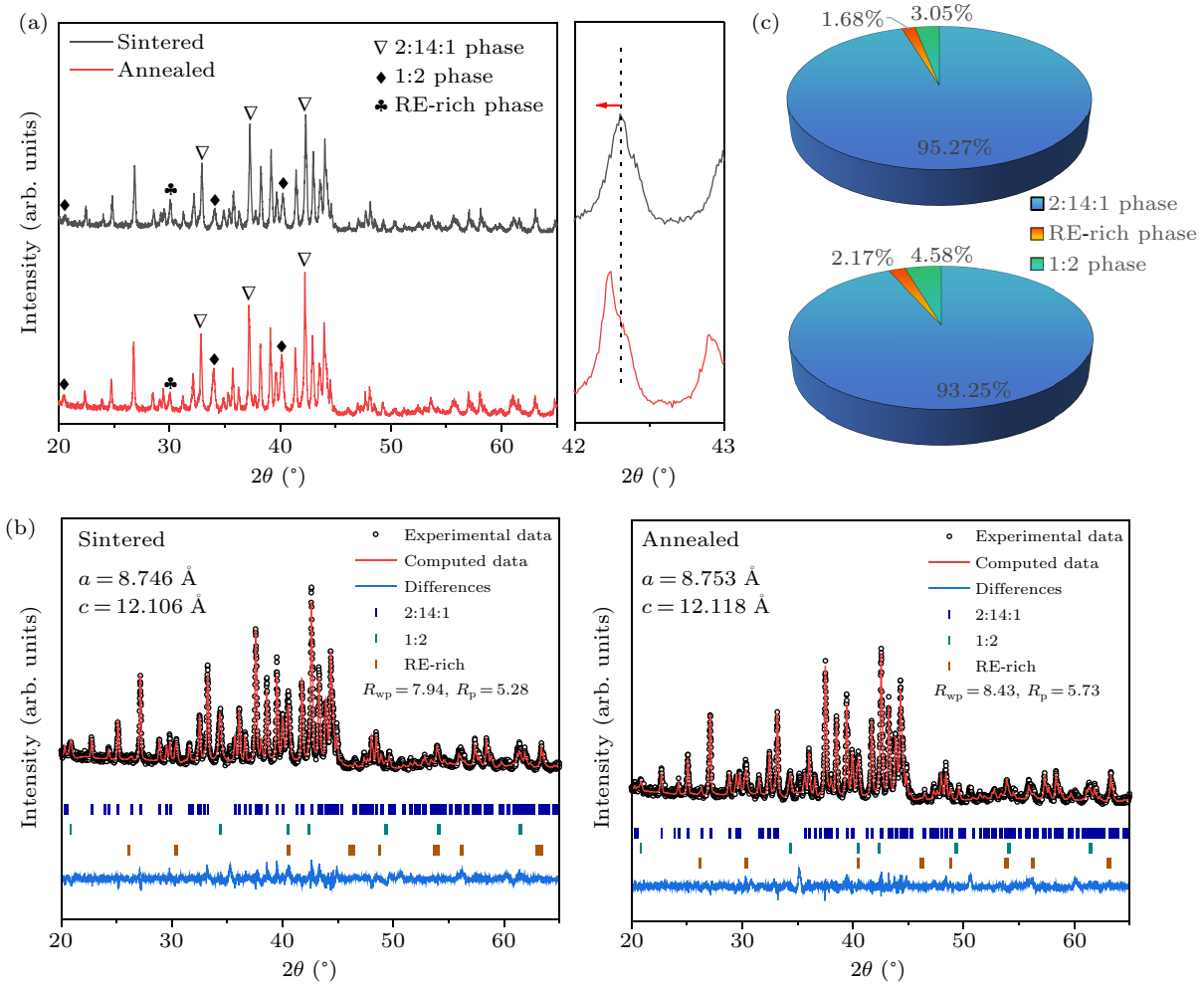


Fig. 2. (a) XRD patterns and local magnification for the powder samples of sintered and annealed Co22 magnets. (b) The refined lattice parameters a and c, observed patterns, calculated patterns and both differences for sintered and annealed samples are given in black, red, and blue colors. (c) The fraction of constituent phases for sintered and annealed Co22 samples.

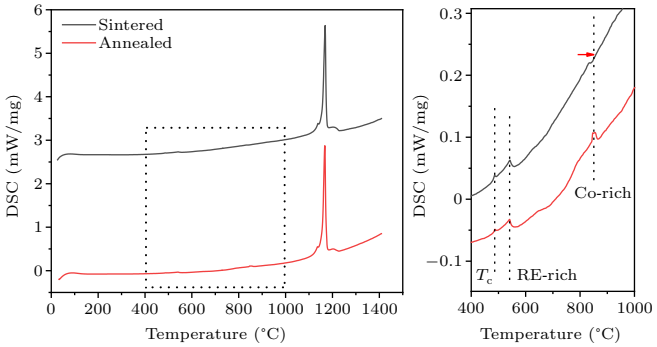


Fig. 3. DSC curves and local magnification of sintered and annealed Co22 samples.

As previously mentioned, it was proven that the redistribution of phase content occurred after annealing, which ultimately affected the magnetic properties. In order to understand the coercivity mechanism in high-Co-containing magnets in depth, it was necessary to investigate the basic physical properties of these constituent phases, especially the newly emerging Co-rich phase. Figure 3 shows the differential thermal analysis curve of Co22 magnets under different heat-treated states. The melting points of each phase were characterized by these protruding peaks. It is obvious that the highest and most prominent peak represents the melting heat absorption of main phase, and the other three small peaks shown in magnification correspond to the curie temperature, RE-rich and Co-rich melting points. respectively. The Curie temperature of Co22 samples is as high as 486 °C due to a lot of Co entering the main phase, which is the fundamental reason for its higher temperature stability. Generally, the melting point is closely related to the phase composition, and the level of the endothermic peak represents the phase content. There is no difference in the melting temperature of RE-rich phase between sintered and annealed samples, which is about

540 °C. Nevertheless, the melting points of Co-rich phase in sintered and annealed magnets are 833 °C and 851 °C, respectively. Both increased melting temperature and distinct peak shape of Co-rich phase indirectly indicated that its composition changes while its content increases slightly.

Figures 4(a) and 4(b) depict the cross-sectional morphologies of Co22 magnets before and after annealing. It is clearly observed that both magnets are composed of the dark gray 2:14:1 main phases, bright white RE-rich phases (marked with a red arrow) and light gray Co-rich phases (marked with a blue arrow). Among them, the two grain boundary phases distributed in blocky morphology are often joined together. It is even difficult to distinguish them with the naked eye in most situations. Combined with energy spectrum analysis as listed in Table 2, it was found that the main difference between RE-rich phase and Co-rich phase is the proportion of ferromagnetic elements. Usually, RE-rich phases containing a low proportion of ferromagnetic elements are nonmagnetic, while Co-rich phase is ferromagnetic due to a higher proportion of ferromagnetic elements. In addition, Co-rich phase was also named as 1:2 phase, because the atomic ratio of rare earth elements to ferromagnetic elements is very close to 1:2. However, in careful comparison with the EDS results, it is found that the proportion of Co in Co-rich phase tends to increase, and the atom ratio of Fe + Co to RE is slightly more than 2 in the annealed samples. It was further proved that the diffusion of Co element to the grain boundary phase did occur during annealing, which may also explain the increasing melting point of Co-rich phase. Figure 5 shows a more detailed nanostructure morphology by TEM. Unexpectedly, isolated spheroid particles were observed in the main phase of annealed samples. The EDS results indicate that these particles enriched in Nd/Pr elements are also RE-rich phase. So far, it has been confirmed that RE-rich phase in annealed samples is composed of two parts. One is distributed at the grain boundaries connecting to Co-rich phase. The other part usually precipitates from the main phase during annealing.

Table 2. The EDS results of RE-rich and Co-rich phases marked in Fig. 4.

Location	Phase	Nd (at%)	Pr (at%)	Tb (at%)	Fe (at%)	Co (at%)	RE/Fe + Co
1	Co-rich	22.6	8.9	0.9	29.5	37.4	1/2.06
2	Co-rich	22.3	9.6	0.4	28.0	36.4	1/1.99
3	Co-rich	23.59	10.54	0.3	29.61	35.96	1/1.92
4	RE-rich	64.6	21.0	6.8	5.0	1.7	13.79/1
5	Co-rich	21.3	9.2	0.6	29.0	39.8	1/2.21
6	Co-rich	20.8	8.1	0.2	34.4	36.6	1/2.44
7	Co-rich	18.7	7.4	0.7	37.3	34.6	1/2.68
8	RE-rich	58.1	19.3		2.9	1.4	18/1

Based on the previously mentioned situation of phase variation, the evolution of the phase structure during annealing is explored in detail. It is worth noting that the melting point of the Co-rich phase is much higher than that of the RE-rich phase. According to DSC curve, the main phase was mostly solid, while RE-rich and Co-rich phases were totally liquid at the primary annealing temperature of 900 °C. Co and Fe elements at the edge of main phase would diffuse into the surrounding liquid phase, while RE element in the grain boundary phase would spread in the opposite direction due to sufficient concentration gradient. This process would inevitably lead to the reduction of the main phase content. At the same time, an excessive rare earth element is inside the main phase. Moreover, the content of Co and Fe increases while the content of RE decreases in some liquid grain boundary phase, which was transformed into new Co-rich phase, preferentially solidified with the original Co-rich phase after subsequent cooling process. Obviously, part of original RE-rich phase was transformed into new Co-rich phase, which contained slightly higher Co content. The variation in the Co-rich phase constituent of the annealed sample also explained the difference of peak pattern in DSC curve.

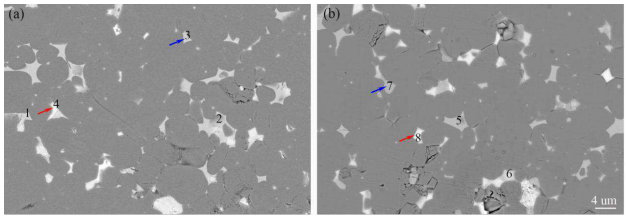


Fig. 4. SEM images of (a) sintered and (b) annealed Co22 samples.

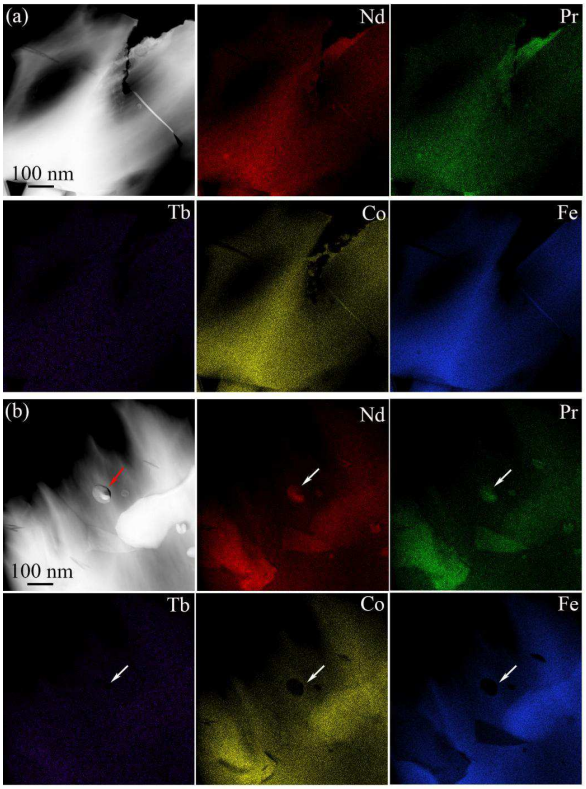


Fig. 5. HAADF images and the corresponding STEM-EDS mapping for Nd, Pr, Tb, Co and Fe elements of (a) sintered and (b) annealed Co22 samples.

At the second annealing temperature, only RE-rich phase was still liquid while the main phase and Co-rich phase were already solid. In this process, RE-rich phase structure is mainly adjusted. On the one hand, the preferential solidified Co-rich phase at the grain boundary prevented RE-rich phase from forming an isolation layer to wrap the main phase. On the other hand, saturated RE elements would directly precipitate from the main phase in the form of spherical particles. It is summarized that the thermal diffusion of Co (Fe) and RE elements along the opposite direction occurred in the heating and holding process, which resulted in the adjustment of grain boundary phase distribution after cooling. Eventually, the content of both grain boundary phases increased after second annealing. The results indicated that the microstructure of high-Co-containing magnets is completely different from that of conventional Nd–Fe–B magnets.

It is well known that the coercivity is usually affected by low-temperature annealing in conventional Nd–Fe–B magnets, in which the optimization of grain boundary phase morphology is crucial for improving magnetic properties. However, the nonmagnetic RE-rich phase of high-Co-containing magnets was distributed at both the grain boundary and the main phase. The effective magnetic isolation layer was not formed due to the morphology of large block distribution and spherical particles. On the contrary, the coupling effect between the main phase was enhanced because of ferromagnetic Co-rich phase at the grain boundary. The increasing ferromagnetic phase is the reason for the deterioration of the magnetic properties. It is worth noting that the coercivity was obviously affected by the second annealing temperature according to Fig. 1(b), while the second annealing process is mainly related to the distribution of RE-rich phase. It was confirmed that RE-rich phase played a certain role in coercivity of annealed high-Co-containing magnets. The mechanism of coercivity formation needs further investigation.

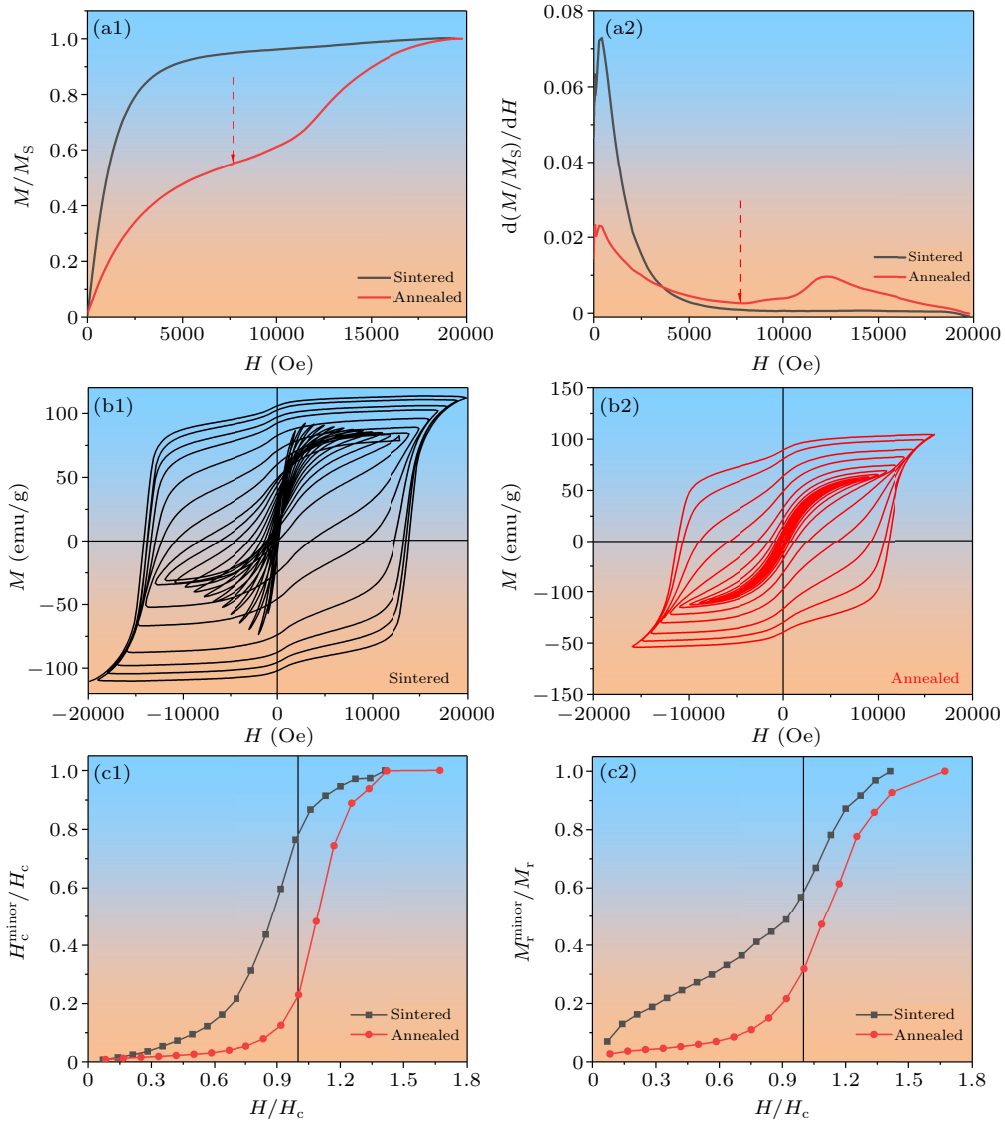


Fig. 6. Room temperature out-of-plane normalized initial magnetization curves (a1) and the corresponding first derivative curves (a2) of sintered and annealed Co22 samples, Minor hysteresis loops of Co22 samples in sintered (b1) and (b2) annealed states, normalized coercivity (c1) and normalized remanence (c2) with the normalized external magnetic field.

Usually, the initial magnetization curve had an important effect on explaining the magnetization reversal of permanent magnet materials. Figure 6(a1) shows the dependence of the normalized initial magnetization curve on different heat-treated state, which starts at the thermally demagnetized state. The corresponding first-order derivatives were also indicated in Fig. 6(a2). The sintered samples showed a relatively large susceptibility which is similar to that of conventional Nd–Fe–B magnet. At a low magnetic field, sintered samples magnetized rapidly from 0 T to 0.3 T and a slow magnetization process occurred from 0.3 T to 2 T, which shows a very steep slope and then slope decreases significantly in the first-order derivative curve. This steep initial magnetization curve indicates that its magnetization reversal is mostly controlled by nucleation, in which the domain wall motion is easy. However, an S-shaped two-stage magnetization was observed in annealed magnets. It started with high-susceptibility region to the magnetic field of 0.7 T and then changed to relatively lower susceptibility. After reaching a critical field, it again possessed a sharp rise. As a result, the presence of minimal values was seen in the corresponding first-order derivative curves, as shown in Fig. 6(a2). Such a step-behavior curve indicates that annealed sample shows signs of domain wall pinning during magnetization.[29] The initial high susceptibility meant that the domain wall first moved freely within the grains, which is similar to that of sintered samples. Then, the decrease in susceptibility suggests that some of the domain walls in the thermally demagnetized stage are obviously pinned. Thus, a higher magnetic field is required to magnetize. After the depinning of the magnetic domain walls, the susceptibility continued increasing to the saturation magnetization. The depinning fields for the annealed samples were about 1.2 T, as seen from Fig. 6(a1). It is evident that the internal interaction of the material changes significantly under different heat-treated states. The minor hysteresis loops in Figs. 6(b1) and 6(b2) can be used to reflect the gradual magnetization process. These minor hysteresis loops are composed of a group of loops with the magnetic field less than the saturation field. Figure 6(c1) shows the coercivity H_{cminor} of each minor loop as a function of magnetic field H, where the horizontal and vertical coordinates are normalized with respect to H_{c}. When $H/H_{\mathrm{c}} = 1$, the H_{cminor} in sintered sample has reached 78% of its maximum coercivity, and rapidly reaches the maximum value with the external field increases. In this case, the nucleation and expansion of reversed domains are the main mechanisms controlling the demagnetization process. However, H_{cminor} in annealed sample is only 22% of its maximum coercivity when $H/H_{\mathrm{c}} = 1$, and increases slightly slowly. The variation trend of the normalized remanence $M_{\mathrm{rminor}}/M_{\mathrm{r}}$ is similar to that of $H_{\mathrm{cminor}}/H_{\mathrm{c}}$ as shown in Fig. 6(c2), indicating that the coercivity of the annealed samples is controlled by both nucleation and pinning, which is consistent with the results of the initial magnetization curves.

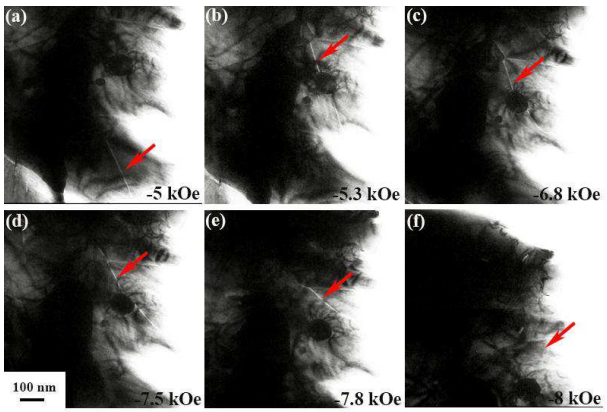


Fig. 7. (a)–(f) Dynamic observation of domain wall movement in the region around quasi-circular phase by Lorentz transmission electron microscope with increased external field.

In order to observe the pinning effect in an intuitive way, Lorentz transmission electron microscope (LTEM) was used to track the domain motion in annealed magnets. Figures 7(a)–7(f) show the magnetization reversal process under different external magnetic fields. In the beginning, the domain walls move easily almost without hindrance. As the applied field increased, evident phenomenon of domain wall pinning appeared in the annealed sample. When the applied magnetic field is large enough, the domain walls can be depinned. It is found that the center of the pinning is a quasi-circular phase. Combined with EDS results in Fig. 5(b), it is confirmed that RE-rich particle precipitated from the main phase would become the later pinning center. It is interesting that different coercivity mechanism appeared depending on heat-treated process in high-Co-containing magnets. In fact, the existence of Co-rich phase has an important effect on phase redistribution after annealing, which eventually leads to different demagnetization behavior. That is, the coercivity of sintered samples is still controlled by single nucleation, while it is determined by both nucleation and pinning in annealed samples.

Combined with coercivity mechanism mentioned above, their magnetic properties in high-Co-containing magnets were discussed with different heat-treated states. Due to the lessened content of the 2:14:1 main phase, the remanence B_{r} decreased a bit in the annealed magnets. However, the influencing factors of coercivity are slightly complicated. On the one hand, part of the nonmagnetic RE-rich phase was transformed into ferromagnetic Co-rich phase, and the direct increase of magnetic phase at the grain boundary significantly weakened the isolation between the main phase. Once the magnetization reversal domain appeared, it was easier to expand rapidly under the control of nucleation mechanism, resulting in significant decrease in coercivity. On the other hand, nonmagnetic RE-rich particles precipitated from the main phase acting as the pinning center in annealed high-Co-containing magnets, effectively inhibiting the magnetic domain motion, which may be beneficial to improve coercivity under the control of pinning mechanism. Considering the synergistic effect of mixed

mechanism, the emergence of the pinning phenomenon effectively offset part of the reduction in coercivity due to enhanced exchange coupling. Therefore, the limited reduction of about 1.8 kOe was found in annealed high-Co-containing magnets. For the annealed magnets in this paper, increased ferromagnetic phase interfaces provided a large number of nucleation sites, which plays a dominant role in coercivity. However, regulating the second annealing temperature affected the distribution of RE-rich phase directly, especially the spheroid RE-rich particle precipitation from the main phase. The resulting pinning effect is changed, and then the coercivity is also affected. The variation of coercivity in high-Co-containing magnets with second annealing temperature further confirmed the existence of pinning mechanism. In other words, exploring the appropriate heat-treated schedule to improve the pinning effect would be crucial for improving coercivity of high-Co-containing magnets.

4. Conclusion

In this work, the microstructure and magnetic properties of high-Co containing magnets with high thermal stability under different heat-treated conditions have been systematically studied. The results show that sintered magnets were mainly composed of hard magnetic 2:14:1 main phase, ferromagnetic Co-rich phase with high melting point and nonmagnetic RE-rich phase with low melting point. Among these, the two grain boundary phases were almost connected together and distributed in blocky form at the grain boundary. After annealing, both the content and distribution of constituent phase were adjusted in high-Co containing magnets. On the one hand, the decrease of main phase content was accompanied by the increase of the content of the other two grain boundary phases. On the other hand, a small amount of RE-rich phase with the morphology of spherical particles precipitated from the main phase in addition to that distributed at the grain boundary.

For high-Co containing magnets, the regulation of microstructure eventually led to different coercivity mechanisms between sintered and annealed magnets. The former is controlled by a single nucleation, while the latter is controlled by both nucleation and pinning. After annealing, the increase of ferromagnetic Co-rich grain boundary phase further enhanced the contact of main phase, which caused a significant reduction in coercivity. However, the newly precipitated spherical RE-rich particles would become the nailing center of the domain wall, which hindered the movement of domain wall during the process of reverse magnetization. The emergence of the pinning effect certainly contributed to the improvement of the coercivity. Eventually, the strengthening effect of pinning partially compensated for the weakening effect of magnetic isolation, and the coercivity of annealed high-Co containing magnets in this paper appeared to decrease moderately. The essence of improving coercivity by optimizing the second annealing temperature is to obtain the maximum pinning effect. Our results are expected to provide important references for understanding the magnetic mechanisms in high-Co containing magnets and designing high-performance magnets.

Acknowledgments

Project supported by National Key R&D Program of China (Grant No. 2021YFB3803003) and Youth Innovation Promotion Association CAS (Grant No. 2023311).

References

[1] Matsuura Y 2006 *J. Magn. Magn. Mater.* **303** 344
[2] Gutfleisch O, Willard M A, Brück E, Chen C H, Sankar S G and Liu J P 2011 *Adv. Mater.* **23** 821
[3] Coey J M D 2020 *Engineering* **6** 119
[4] Prashanth N A 2022 *Mater Today: Proc* **49** 731
[5] Li Y H, Fan X D, Jia Z, Fan L, Ding G F, Liu X C, Guo S, Zheng B, Cao S, Chen R J and Yan A R 2024 *Chin. Phys. B* **33** 037508
[6] Sepehri-Amin H, Hirosawa S and Hono K 2018 *Handb. Magn. Mater.* **27** 269
[7] Skokov K P and Gutfleisch O 2018 *Scr. Mater.* **154** 289
[8] Sagawa M, Hirosawa S, Yamamoto H, Fujimura S and Matsuura Y 1987 *J. Appl. Phys.* **26** 785
[9] Hirosawa S, Matsuura Y, Yamamoto H, Fujimura S, Sagawa M and Yamauchi H 1986 *J. Appl. Phys.* **59** 873
[10] Sinnema S, Radwanski R J, Franse J J M, de Mooij D B and Buschow K H J J 1984 *Magn. Magn. Mater.* **44** 333
[11] Zhou S Z, Guo C J, Hu Q and Li C H 1988 *Journal of Beijing University of Iron and Steel Technology* **10** 317
[12] Li W, Jiang L, Wang D W, Sun T D and Zhu J H 1986 *J. Less-Common. Met.* **126** 95
[13] Mottram R S, Williams A J and Harris I R 2000 *J. Magn. Magn. Mater.* **217** 27
[14] Mottram R S, Williams A J and Harris I R 2000 *J. Magn. Magn. Mater.* **222** 305
[15] Li D, Dong S Z and Xu J Y 2021 *Powder Metallurgy Industry* **31** 25
[16] Ding G F, Guo S, Cai L W, Chen L, Yan C J, Lee D and Yan A R 2015 *IEEE Trans. Magn.* **8** 2100504
[17] Zhang J T, Xu J Y, Hu C L, Meng R Y and Dong S Z 2022 *J. Chin. Soc. Rare Earths* **40** 236
[18] Jin M X, Fan S N, Kou M P, Wang H Q, Jia Z, Li Y H, Ding G F, Cao S, Fan X D, Guo S, Chen R J and Yan A R 2023 *J. Alloy Compd.* **943** 169180
[19] Wu Y Y, Skokov K P, Schäfer L, Maccari F, Aubert A, Rao Z Y, Schweinar K, Gault B, Xu H, Jiang C B and Gutfleisch O 2022 *Acta Mater.* **240** 118311
[20] Arai S and Shibata T 1985 *IEEE Trans. Magn.* **21** 1952
[21] Xu J Y, Zhang J T, Meng R Y, Chen H S, Fang Y K, Dong S Z and Li W 2023 *Acta Phys. Sin.* **72** 077502 (in Chinese)
[22] Zhang J T, Xu J Y, Jin J Y, Meng R Y and Dong S Z 2022 *Acta Phys. Sin.* **71** 167502 (in Chinese)
[23] Xu J Y, Hu C L, Zhang J T, Dong S Z and Chen H S 2022 *Met. Funct. Mater.* **1** 106
[24] Wu Y Y, Skokov K P, Schäfer L, Maccari F, Aubert A, Xu H, Wu H C, Jiang C B and Gutfleisch O 2022 *Acta Mater.* **235** 118062
[25] Wu Y Y, Skokov K P, Schäfer L, Maccari F, Xu H, Wang X X, Jiang C B and Gutfleisch O 2024 *Acta Mater.* **263** 119517
[26] Huang Q F, Jiang Q Z, Zhong K X, Chen D K, Xu D Q, Shi D W, Fu G, Yan J L, Rehman S U, Ma Q, Liu R H and Zhong Z C 2024 *J. Mater. Sci. Technol.* **181** 63
[27] Pope C G 1997 *J. Chem. Educ.* **74** 129
[28] Yang M N, Wang H, Hu Y F, Yang L Y, Maclennan A and Yang B 2017 *J. Alloy Compd.* **710** 519
[29] Li C H, Zhao X T, Liu L, Liu W, Ye Z X, Wu J X, Li Y, Ma J, Ju H Z, Song Y H and Zhang Z D 2023 *J. Alloys Compd.* **960** 170816